Nikola Mišković, Zoran Vukić, Matko Barišić

Identification of Unmanned Underwater Vehicles by Self-Oscillation Method

Control of underwater vehicles is a challenging task since these systems demonstrate highly coupled and nonlinear behavior in uncertain and often unknown environment. In order to successfully design higher levels of control hierarchy, sufficiently accurate parameters of a mathematical model describing the vessel is required. These parameters vary significantly depending on the payload; hence conventional, time-consuming identification methods are tedious.

This paper introduces a self-oscillation based method for determining inertia and drag parameters for underwater vehicles. The procedure is easily implementable in field conditions and gives satisfactory results. Both linear and nonlinear models of yaw, heave and surge degree of freedom can be identified. Experimental results obtained from yaw identification experiments on a real underwater vehicle will be presented. In addition to this, the same methodology will be used to determine which model describes the vehicle dynamics more suitably. Modifications of the proposed algorithm for systems with delays and discrete-time systems will be described, together with an estimate of parameter error bounds due to quantization levels.

Key words: Nonlinear systems, Unmanned underwater vehicles, Identification, Self-oscillations

Identifikacija bespilotnih ronilica korištenjem postupka vlastitih oscilacija. Upravljanje bespilotnim ronilicama predstavlja zahtjevan zadatak budući da ronilice pokazuju snažno spregnuto i nelinearno ponašanje u nepredvidljivim i često nepoznatim okruženjima. U svrhu uspješnog projektiranja viših razina u njihovoj upravljačkoj hijerarhiji, potrebno je dovoljno dobro poznavati parametre matematičkog modela plovila. Ovi se parametri mogu znatno mijenjati ovisno o opremi i drugim uvjetima tijekom misije, stoga su uobičajeni, vremenski zahtjevni identifikacijski postupci neprikladni.

Članak opisuje postupak koji koristi vlastite oscilacije za određivanje inercije i otpornosti bespilotnih ronilica. Postupak je lako primjenjiv u terenskim uvjetima i daje zadovoljavajuće rezultate. Linearan i nelinearan model zaošijanja, zaranjanja i napredovanja moguće je identificirati. U radu su prikazani eksperimentalni rezultati dobiveni na identifikacijskim ekperimentima zaošijanja na stvarnoj ronilici. Uz navedeno, ista metodologija je iskorištena za odlučivanje o modelu koji prikladno opisuje stvarnu ronilicu. U radu su opisane i preinake predloženog algoritma za sustave s transportnim kašnjenjem i diskretne sustave, kao i procjene pogrešaka u određivanju parametara koje su posljedica kvantizacije.

Ključne riječi: nelinearni sustavi, bespilotne ronilice, identifikacija, vlastite oscilacije

1 INTRODUCTION

Underwater robotics is an area that occupies interest of the research community increasingly over the years. The main reason for this is probably the ever growing number of applications of these technologies in real life. Underwater vehicles (UVs) are widely used in marine biology, underwater archeology, navies, hydrography, oceanography, fishery, etc. These vehicles can be divided into remotely operated vehicles (ROVs) whose main characteristic is that they are controlled from the surface via tether; and autonomous underwater vehicles (AUVs) which act as autonomous systems without any communication with the surface. There are many commercial ROVs available on the market (VideoRay, Seamor, Benthos, etc.) and the market of AUVs has started to grow in the last few years (IVER2, Remus, etc.). The applications of these vehicles vary from underwater cartography to military applications (mine detection and disposal).

From the control point of view, AUVs require much more effort in control design. In general, control strategies for marine vehicles can be divided into three levels. The low level is responsible for control of the vehicles' speeds (surge, yaw rate, etc.), positions (depth, dynamic

positioning, etc.) and orientations (heading, tilt angle, etc.), [2], [8]. Mid level of control is responsible for path following, trajectory tracking and gives commands to the low level, [4]. High level of control is dedicated to mission management, mission planning (path and trajectory planning) and to safety issues (collision avoidance, fault tolerance, etc.), [19]). For a higher level to function properly, low levels have to be designed and work reliably. In order to design the low level control structure, UV mathematical model parameters have to be identified.

Many identification procedures applicable to marine vehicles can be found in the literature, only few will be mentioned in this paper. In order to identify mathematical model parameters of an underwater vehicle, different sensors can be used, such as inertial measurement units (IMUs), Doppler velocity loggers (DVLs), ultrashort baseline positioning systems (USBLs), etc., [3]. In research community, vision-based techniques are widely used, probably due to low cost. These techniques determine the position of an UV using a camera, and this data is then further processed to calculate higher order derivatives and thus dynamic model parameters. An interesting vision-based laboratory apparatus used for URIS ROV parameter identification was described in [20]. It was based on placing a floor pattern at the bottom of the laboratory pool enabling the position of the vehicle to be uniquely determined by the help of the onboard down facing camera. Another approach found in the literature is to use an external camera with perspective view placed next to the pool, [6]. The authors have implemented a similar technique with a camera placed exactly above the laboratory swimming pool, obtaining orthogonal view from above on the vehicle, [15].

The above mentioned methodologies and apparatus allow application of classical process identification methods, [12]. These methods require time consuming experiments, great number of collected data and computations of high complexity, and can be quite tedious and impractical in situations where sensor suite of the ROV changes. The parameters of the mathematical model of the vehicle also change significantly and, unless this model was identified previously, heading and depth controllers will not behave in a satisfactory manner. Different payload can be mounted on an UV (CTD probes, side-scan sonars, acoustic modems, etc.), depending on the application, and every time the model parameters will change. Performing conventional identification methods is not possible in these cases, and a need for a quick, feasible in the field, easily implementable method is required.

One of such methods has been used for surface marine vehicles and is called the "zig-zag" test. The "zig-zag" maneuver has been used for designing ship autopilots, i.e. determining yaw motion of a surface vessel, [13]. The ma-

noeuvre consists in turning the ship rudder at the maximum speed to the starboard side at $10°$ $(20°)$; when ships course changes by $10°$ $(20°)$ from the initial course, the rudder is turned to the opposite side (port) at $10°$ $(20°)$, causing the ship to turn to port. When ship course changes by $10°$ $(20°)$ from the initial course on the opposite side, the rudder is again turned to the starboard side at $10°$ $(20°)$. The heading and the rudder position are recorded all the time during the experiment. Under the assumption that the ship yaw model can be described with a linear first order astatic differential equation (Nomoto model), the obtained data can be integrated and model parameters can be explicitly determined. This procedure is practical if linear Nomoto model describes the vessel's dynamic properly. However, if nonlinear terms in the drag appear, the procedure cannot be used. This method is not robust to external disturbances, [16], and a great number of sequential data have to be integrated to calculate the parameters.

This paper will present a method which uses similar oscillating data as in the "zig-zag" test, only it uses simpler calculations to determine the model parameters. It is based on the describing function method, [18], [23], and can therefore be used to determine nonlinear model parameters, also. The paper is organized as follows. Section 2 describes mathematical models of underwater vehicles and presents their simplifications that are used for control purposes. In Section 3 a theoretical approach to self-oscillations is given, together with proofs of self-oscillation symmetry for astatic systems. Section 4 describes the proposed identification by use of self-oscillations (IS–O) method and presents complete formulae for calculating unknown parameters in two case studies, which are used to describe the dynamics of underwater vehicles. Section 5 describes how IS–O method can be applied to underwater vehicles and gives experimental results obtained on a real ROV. The paper is concluded with Section 6.

2 UNDERWATER VEHICLES' MATHEMATICAL MODELS

In order to define the full mathematical model of a general marine vehicle the terminology adopted from [7] will be used. First of all, two coordinate frames should be defined: an Earth-fixed coordinate system {E} which is steady, immobile coordinate frame, and a body-fixed coordinate system {B}, which is usually attached to the centre of gravity (CG) of the vehicle, as shown in Fig. 1. Variables that are included in the mathematical model of marine vehicles are linear and angular velocities, positions and orientations, and forces that excite the vehicle. These are listed in Table 1 together with their names, which are common in marine applications. Surge, sway and heave

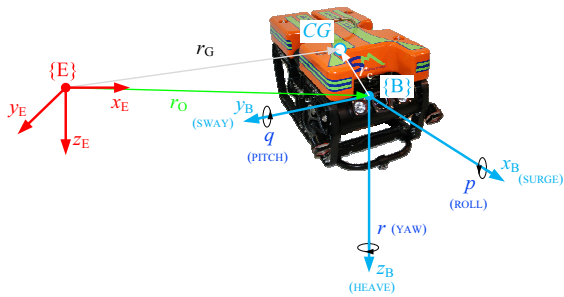| DOF	surge	sway	heave	roll	pitch	yaw	defined in
$\boldsymbol{\nu}$	u	v	w	p	q	r	{B}
$\boldsymbol{\eta}$	x	y	z	φ	θ	ψ	{E}
$\boldsymbol{\tau}$	X	Y	Z	K	M	N	{B}

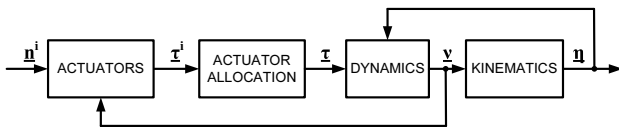*Fig. 1. Body-fixed and Earth-fixed coordinate frames*

Fig. 2. Block-diagram of a complete mathematical model

are defined as motion in the x–, y– and z–direction, respectively, while roll, pitch and yaw are defined as rotation about x–, y– and z–axis, respectively.

Earth-fixed coordinate system {E} is used to define vehicle's positions $\boldsymbol{\eta}_1 = \begin{bmatrix} x & y & z \end{bmatrix}^T$ and orientations $\boldsymbol{\eta}_2 = \begin{bmatrix} \varphi & \theta & \psi \end{bmatrix}^T$ forming a six element vector $\boldsymbol{\eta} = \begin{bmatrix} \boldsymbol{\eta}_1^T & \boldsymbol{\eta}_2^T \end{bmatrix}^T$. In the same manner, body-fixed coordinate frame is used to define linear velocities $\boldsymbol{\nu}_1 = \begin{bmatrix} u & v & w \end{bmatrix}^T$ (surge, sway and heave), and rotational velocities $\boldsymbol{\nu}_2 = \begin{bmatrix} p & q & r \end{bmatrix}^T$ (roll, pitch and yaw) forming a six element vector $\boldsymbol{\nu} = \begin{bmatrix} \boldsymbol{\nu}_1^T & \boldsymbol{\nu}_2^T \end{bmatrix}^T$.

Motion of the vehicle is achieved by applying external forces and moments. Three forces (each in the direction of one body-fixed frame axis) and three moments (defined as rotation about each body-fixed frame axis) form a six element vector of external forces and moments in the form $\boldsymbol{\tau} = \begin{bmatrix} X & Y & Z & P & Q & R \end{bmatrix}^T$. External forces are exerted by actuators. Let τ^i denote commanded thrusts for each actuator ($i = 1, \ldots, n$ where n is the number of actuators). Value n^i denotes commanded inputs for the actuators themselves (rotation speed of the propeller, rudder deflection, etc.). Using this notation, the complete mathematical model can be represented with Fig. 2.

Actuators

Actuators in technical systems are actuating devices that perform desired action on the system, [22]. In marine systems these are roughly divided into thrusters (propulsors), control surfaces and mass. This paper will focus on underwater vehicles with thrusters.

As the thruster i rotates, it exerts thrust τ^i and torque q^i which can be described with (1) where n is propeller revolution rate and $T_{n|n|}$, $T_{|n|u_a}$, $Q_{n|n|}$ and $Q_{|n|u_a}$ are positive coefficients given by the propeller characteristics. This model is also known as the *bilinear thruster model*, [7].

$$\begin{aligned} \tau^i &= T_{n|n|}n\,|n| - T_{|n|u_a}\,|n|\,u_a \\ q^i &= Q_{n|n|}n\,|n| - Q_{|n|u_a}\,|n|\,u_a \end{aligned} \tag{1}$$

A simpler model given with (2) can be derived if ambient water speed u_a (see [19]) is neglected.

$$\tau^i = a\,|n|\,n + bn. \tag{2}$$

This model is more applicable in practice especially at low speeds. Further simplification gives that linear part of the model can also be neglected, i.e. $b = 0$, giving the so called *affine model*.

However, the force exerted by thrusters is rarely the same when the propeller is rotating clockwise and counterclockwise. This is why a more complex model given with (3) should be used. Subindices f and b denote 'forward' and 'backward'.

$$\tau^i = \begin{cases} a_f\,|n|\,n + b_f n, & n > 0 \\ a_b\,|n|\,n + b_b n, & n < 0 \end{cases} \tag{3}$$

The influence of the torque exerted by a thruster can be compensated if thrusters are positioned in pairs in such a way that they are counter-rotating.

Actuator allocation

Actuator allocation is a linear connection between the space of actuator forces (described with vector $\boldsymbol{\tau}^i$) and the space of vehicle's forces and moments (described with vector $\boldsymbol{\tau}$). The matrix which describes this link is called the *allocation matrix* and it depends on the number of available actuators and their topology.

Kinematic model

Kinematic model gives the relation between the speeds ν in a body-fixed coordinate frame {B} and first derivative of positions and angles η in an Earth-fixed coordinate system {E}. A full set of kinematic equations is given with (4)

$$\begin{bmatrix} \dot{\eta}_1 \\ \dot{\eta}_2 \end{bmatrix} = \begin{bmatrix} \mathbf{J}_1(\eta_2) & \mathbf{0}_{3\times 3} \\ \mathbf{0}_{3\times 3} & \mathbf{J}_2(\eta_2) \end{bmatrix} \begin{bmatrix} \nu_1 \\ \nu_2 \end{bmatrix} \Leftrightarrow \dot{\eta} = \mathbf{J}(\eta)\nu$$

$$\tag{4}$$

where

$$\mathbf{J}_1(\eta_2) = \begin{bmatrix} c\psi c\theta & -s\psi c\phi + c\psi s\theta s\phi & s\psi s\phi + c\psi s\theta c\phi \\ s\psi c\theta & c\psi c\phi + s\psi s\theta s\phi & -c\psi s\phi + s\psi s\theta c\phi \\ -s\theta & c\theta s\phi & c\theta c\phi \end{bmatrix}$$

and

$$\mathbf{J}_2(\eta_2) = \begin{bmatrix} 1 & s\phi t\theta & c\phi t\theta \\ 0 & c\theta & s\phi \\ 0 & s\phi c^{-1}\theta & c\phi c^{-1}\theta \end{bmatrix}.$$

For the sake of brevity, c denotes cosine, s sine, t tangent and superscript -1 is the reciprocal function.

Dynamic model

The dynamic model gives relation between velocities ν and accelerations $\dot{\nu}$ of the vehicle and forces τ that act on it, and is highly nonlinear and coupled.

$$\underbrace{(\mathbf{M}_{RB} + \mathbf{M}_A)}_{\mathbf{M}}\dot{\nu} + \underbrace{(\mathbf{C}_{RB}(\nu) + \mathbf{C}_A(\nu))}_{\mathbf{C}(\nu)}\nu$$
$$+ \mathbf{D}(\nu)\nu + \mathbf{g}(\eta) = \tau + \tau_E \tag{5}$$

A full dynamic equation of forces acting on marine vehicles can be written in a compact form given with (5) where $\mathbf{M}_{RB}$ is a rigid-body inertia matrix, $\mathbf{C}_{RB}$ is the rigid-body Coriolis and centripetal matrix, $\mathbf{M_A}$ is added-mass matrix, $\mathbf{C_A}(\nu)$ is added-mass Coriolis and centripetal matrix, $\mathbf{D}(\nu)$ is total hydrodynamic damping matrix, and they are all 6 by 6 matrices. $\mathbf{g}(\eta)$ is vector of restoring forces, τ_E is the vector of environmental forces and moments (waves, winds, current) and τ is the vector of actuation forces and moments. The latter three vectors have dimensions 6 by 1, [7], [19].

2.1 Uncoupled model for underwater vehicles

Coupling effects in (5) can appear for the following reasons:

- existence of coupled terms in the added mass matrix $\mathbf{M}_A$ (nondiagonal terms),

- existence of Coriolis and centripetal forces and

- difference between the center of gravity and the origin of the body-fixed coordinate frame.

The first reason is almost always neglected because these coupling terms have insignificant influence on the behavior of the vehicle, [7]. If it is assumed that the vehicle is moving at slow speed, the effect of Coriolis and centripetal forces can also be neglected. This simplification is usually performed in modeling underwater vehicles, [20]. Incongruity of the center of gravity and the origin of the body-fixed coordinate system can be neglected in underwater vehicles of smaller dimensions [15]. Having this in mind, the simplifications which are introduced in order to obtain an uncoupled model for underwater vehicles are:

- coupled added mass terms are negligible,

- center of gravity CG coincides with the origin of the body-fixed coordinate frame B,

- roll and pitch motion are negligible, i.e. $\varphi = \theta = p = q = 0$.

As a consequence of these simplifications

- total mass matrix $\mathbf{M}_{RB} + \mathbf{M}_A$ is diagonal,

- the total Coriolis and centripetal matrix $\mathbf{C}_{RB}(\nu) + \mathbf{C}_A(\nu)$ vanishes, and

- restoring forces influence only the heave degree of freedom.

These simplifications lead to one, generalized, uncoupled, nonlinear dynamic equation that describes surge, sway, heave ad yaw degree of freedom separately and it is given with

$$\alpha_\nu \dot{\nu}(t) + \beta(\nu(t)) \cdot \nu(t) = \delta + \tau(t). \tag{6}$$

Parameters $\nu(t)$, $\tau(t)$, δ, α and $\beta(x(t))$ are interpreted in Table 2 for each degree of freedom, where τ_{XE}, τ_{YE}, τ_{ZE} and τ_{NE} represent external disturbances, W is weight of the vehicle and B is vehicle's buoyancy. Other vehicle parameters notations have been taken from [7] and are widely used in literature.

3 SELF-OSCILLATIONS

One of the many behaviors that nonlinear systems exhibit is called *limit cycle*, [23], [21]. During this state, the closed-loop system state trajectories form a closed curve (limit cycles). In the time domain, this behavior is represented as oscillatory behavior. The oscillations which arise as a consequence are called *self-oscillations* (S-O).

Table 2. Parameters in (6) depending on the DOF.

DOF	$\nu(t)$	α_ν	$-\beta(\nu(t))$	δ	$\tau(t)$
surge	u	$m - X_{\dot{u}}$	$X_u + X_{u\|u\|}\|u\|$	τ_{XE}	X
sway	v	$m - Y_{\dot{v}}$	$Y_v + Y_{v\|v\|}\|v\|$	τ_{YE}	Y
heave	w	$m - Z_{\dot{w}}$	$Z_w + Z_{w\|w\|}\|w\|$	$\tau_{ZE} + W - B$	Z
yaw	r	$I_r - N_{\dot{r}}$	$N_r + N_{r\|r\|}\|r\|$	τ_{NE}	N

The fact that the closed-loop system is in steady oscillations does not imply that it is on the edge of stability. The self-oscillations are a stable, controlled behavior characteristic for nonlinear systems, unlike steady oscillations that arise in linear time-invariant systems on the border of stability, [22].

3.1 Describing function

Harmonic linearization is a tool for obtaining an approximation of a nonlinear element in the cases when self-oscillations are present. The describing function is consequently an equivalent gain of a nonlinear element which is excited by periodic signals. Let a biased monoharmonic signal be defined as

$$x(t) = x_0 + X_m \sin \omega t = x_0 + x^* \qquad (7)$$

and let it be placed at the input of a nonlinear element whose output is then in the form

$$y_N(t) = F(x). \qquad (8)$$

The output $y_N(t)$ of the nonlinear element $F(x)$ can be developed into a Fourier series

$$y_N(t) = Y_0 + \sum_{k=1}^{\infty} Y_{Pk} \sin(k\omega t) + \sum_{k=1}^{\infty} Y_{Qk} \cos(k\omega t) \quad (9)$$

where

$$
\begin{aligned}
Y_0 &= \frac{1}{2\pi} \int_0^{2\pi} F(x_0 + X_m \sin \omega t) d(\omega t) \\
Y_{Pk} &= \frac{1}{\pi} \int_0^{2\pi} F(x_0 + X_m \sin \omega t) \sin(k\omega t) d(\omega t) \\
Y_{Qk} &= \frac{1}{\pi} \int_0^{2\pi} F(x_0 + X_m \sin \omega t) \cos(k\omega t) d(\omega t).
\end{aligned}
\qquad (10)
$$

If only the first harmonic is taken into account, (9) is simplified into

$$
\begin{aligned}
y_N(t) &= Y_0 + Y_{P1} \sin \omega t + Y_{Q1} \cos \omega t = \\
&= Y_0(x_0, X_m) + \left[\frac{Y_{P1}(x_0, X_m)}{X_m} + \frac{Y_{Q1}(x_0, X_m)}{X_m} \frac{p}{\omega} \right] x^*
\end{aligned}
\qquad (11)
$$

where $p = \frac{d}{dt}$ is the differential operator.

The basic definition of the describing function is formed on symmetric input oscillations. For the symmetric nonlinear element, $F(x) = -F(-x)$, and unbiased oscillations at the input the following expression for the output of the nonlinear element can be written as

$$
\begin{aligned}
y_N(t) &= Y_{P1} \sin \omega t + Y_{Q1} \cos \omega t = \\
&= \left[\frac{Y_{P1}(X_m)}{X_m} + \frac{Y_{Q1}(X_m)}{X_m} \frac{p}{\omega} \right] x^*
\end{aligned}
\qquad (12)
$$

from where the following definition is stated.

Definition 1 (Describing function) *The describing function of a nonlinear element is defined as the ratio between the first harmonic of output and input signals expressed in complex form:*

$$G_N(X_m) = P_N(X_m) + jQ_N(X_m) \qquad (13)$$

where

$$
\begin{aligned}
P_N(X_m) &= \frac{Y_{P1}}{X_m} = \frac{1}{\pi X_m} \int_0^{2\pi} F(X_m \sin \omega t) \sin \omega t \, d(\omega t) \\
Q_N(X_m) &= \frac{Y_{Q1}}{X_m} = \frac{1}{\pi X_m} \int_0^{2\pi} F(X_m \sin \omega t) \cos \omega t \, d(\omega t)
\end{aligned}
\qquad (14)
$$

Similarly, the output of a nonlinear element with a biased harmonic input can then be written as

$$F(x) \approx F_0(x_0, X_m) + \left[P_N(x_0, X_m) + Q_N(x_0, X_m) \frac{p}{\omega} \right] x^*. \qquad (15)$$

This definition allows us to define parameters of the describing function parameters of the asymmetrical nonlinear element $F_0(x_0, X_m)$, $P_N(x_0, X_m)$ and $Q_N(x_0, X_m)$.

Theorem 1 (On vanishing even harmonics) *If a nonlinear element described with $y_N(t) = F(x)$ where $F(x) = -F(-x)$ (symmetrical nonlinear characteristic) is excited with an unbiased monoharmonic signal, $x^*(t) = X_m \sin(\omega t)$, output $y_N(t)$ consists of odd multiples of the first harmonic, only.* □
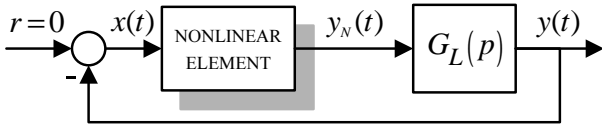
Fig. 3. A closed loop consisting of a nonlinear element and a linear part of the system

Fig. 4. Closed loop system for proving symmetry of self-oscillations with constant input and astatic process

Proof: The simplest way of proving this theorem is to show that even multiples of the first harmonic vanish. In other words, $Y_{P,2k}$ and $Y_{Q,2k}$ have to equal 0.

$$
\begin{aligned}
Y_{P,2k} &= \frac{1}{\pi} \int_0^{2\pi} F\left(x^*\right) \sin\left(2k\omega t\right) d\left(\omega t\right) = \\
&= \frac{1}{\pi} \int_0^{\pi} \left[F\left(x^*\right) - F\left(x^*\right)\right] \sin\left(2k\omega t\right) d\left(\omega t\right) = 0
\end{aligned}
$$

In a similar manner the proof goes for $Y_{Q,2k}$. ∎

3.2 Symmetric self-oscillations

Symmetric oscillations are defined for a closed loop system at the input of the nonlinear element where nonlinear and linear part are separated as shown in Fig. 3, [23], [18]. The input to the system is zero, i.e. $r = 0$. In addition to that, the linear part of the system G_L attenuates higher multiples of the first harmonic of self-oscillations. This is usually achieved in low-pass linear systems. Since most technical systems have low-pass properties, an assumption is made from here on that the higher harmonics are sufficiently attenuated. Given these assumptions, the following set of equations can be written if the system is oscillating at frequency ω:

$$
\begin{aligned}
x\left(p\right) &= -y\left(p\right) \\
y\left(j\omega\right) &= G_L\left(j\omega\right) y_N\left(j\omega\right) \\
y_N\left(j\omega\right) &= G_N\left(X_m\right) x\left(j\omega\right).
\end{aligned}
\tag{16}
$$

These equations boil down to the closed loop equation, which is used to calculate the magnitude X_m and frequency ω of self-oscillations.

$$
G_N\left(X_m\right) G_L\left(j\omega\right) + 1 = 0
\tag{17}
$$

Previously it was assumed that the input to the closed loop system should be 0 for the self-oscillations to be symmetric. The following theorem will show that if the process in the closed loop is astatic (be it linear or nonlinear), the induced self-oscillations will still be symmetric.

Lemma 1 (On symmetric nonlinearities) *Let the nonlinear element be described with $y_N(t) = F(x)$ where $F(x) = -F(-x)$ (symmetrical nonlinear characteristic). If and only if such nonlinear element is excited with an unbiased monoharmonic signal, $x^*(t) = X_m \sin(\omega t)$, Y_0 vanishes.* □
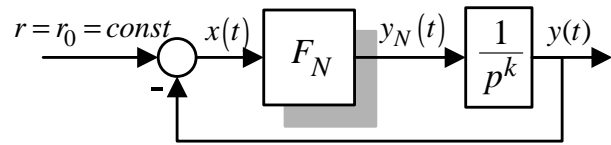
Proof:

⇒ If the nonlinearity is symmetric and the input signal is unbiased then

$$
\begin{aligned}
Y_0 &= \frac{1}{\pi} \int_0^{2\pi} F\left(x^*\right) d\left(\omega t\right) = \\
&= \frac{1}{\pi} \int_0^{\pi} F\left(x^*\right) d\left(\omega t\right) + \frac{1}{\pi} \int_0^{\pi} F\left(-x^*\right) d\left(\omega t\right).
\end{aligned}
$$

Since the nonlinear element is symmetric, $F\left(x\right) = -F\left(-x\right)$, and the proof follows directly as $Y_0 = 0$.

⇐ If $Y_0 = 0$ this means that $\int_0^{2\pi} F\left(x_0 + x^*\right) d\left(\omega t\right) = 0$ from where it follows that

$$
\frac{1}{\pi} \int_0^{\pi} F\left(x\right) d\left(\omega t\right) + \frac{1}{\pi} \int_0^{\pi} F\left(x\right) d\left(\omega t\right) = 0.
$$

Using the property of symmetry,

$$
\frac{1}{\pi} \int_0^{\pi} F\left(x_0 + x^*\right) d\left(\omega t\right) = \frac{1}{\pi} \int_0^{\pi} F\left(-x_0 + x^*\right) d\left(\omega t\right)
$$

which can only be true if $x_0 = -x_0$ from where it follows that $x_0 = 0$.

∎

Theorem 2 (On symmetric S-Os and constant reference) *Let the closed loop system composed of a symmetric nonlinear element and a process as in Fig. 3 be excited with a constant reference signal. If and only if the process is astatic, the induced self-oscillations are symmetric.* □

Proof: Let's say that the process in general is nonlinear and therefore can be joined to the nonlinear part of the system forming a static nonlinearity given with $y_N = F_N(u, \dot{u}, \ddot{u}, \cdots, \dot{y}_N, \ddot{y}_N, \cdots)$ leaving only the k integrators as the linear process as shown in Fig. 4. Let's assume that the input to the nonlinear part is biased, i.e.

that the self-oscillations are asymmetric, $x(t) = x_0 + x^*$. The output of the nonlinear element is then

$$y_N(t) = F_0 + \left[P_N(x_0, X_m, \omega) + \frac{Q_N(x_0, X_m, \omega)}{\omega} p \right] x^*$$
(18)

where the describing function is dependent on the frequency of self-oscillations ω also. The closed loop equations give

$$\begin{array}{l} x = r_0 - y \\ \frac{1}{p^k} y_N = y \\ y_N = F_N(x). \end{array}$$
(19)

Under the assumption that $x(t)$ is biased causing the output of the nonlinear element to be (18), the following equation is obtained:

$$x_0 + x^* = r_0 - \frac{1}{p^k} \left[F_0 + \left(P_N + \frac{Q_N}{\omega} p \right) x^* \right].$$
(20)

The static part of the equation gives that $p^k(x_0 - r_0) = -F_0$.

$\Rightarrow$ Since the process is astatic, $k > 0$, and the k-th derivative of a constant is 0, which implies that $F_0 = 0$. From Theorem 1 it follows that $x_0 = 0$ which proves that the induced S–Os are symmetric.

$\Leftarrow$ If the S–Os are symmetric, $x_0 = 0$ which again according to 1 means that $F_0 = 0$. Then $p^k(-r_0)$ can be equal 0 only if $k > 0$ since the theorem assumption is that $r_0 \neq 0$. This proves that the process is astatic.

∎

3.3 Asymmetric self-oscillations

Asymmetric self-oscillations in general can be a result of a constant input to the system (Theorem 2 proves that this is not the case with any type of closed loop system) or asymmetry in the nonlinear element. The following theorem will show that for astatic systems, self-oscillations are asymmetric if and only if the nonlinear element is asymmetric.

Lemma 2 (On asymmetric nonlinearities) *Let the nonlinear element be described with $y_N(t) = F(x)$ where $F(x) \neq -F(-x)$ (asymmetrical nonlinear characteristic). If and only if such nonlinear element is excited with a biased monoharmonic signal, $x^*(t) = X_m \sin(\omega t)$, Y_0 can vanish.* ☐

Proof: If the nonlinearity is asymmetric and Y_0 can vanish then

$$Y_0 = \frac{1}{\pi} \int_0^{2\pi} F(x_0 + x^*) d(\omega t) = 0.$$

If $x_0 = 0$, Y_0 will never vanish because the nonlinearity is asymmetric. Therefore, it can vanish only if $x_0 \neq 0$, i.e. if the monoharmonic signal is biased. The other direction of the proof is conducted in a similar manner. ∎

Theorem 3 (On asymmetric S–O and nonlinearities)
Let the closed loop system be composed of a nonlinear element and an astatic process. The induced self-oscillations are asymmetric if and only if the nonlinear element is asymmetric. ☐

Proof: As it was shown in the proof of Theorem 2, the closed loop equation can be written using (20) from where it follows that if the process is astatic $F_0 = 0$. According to Lemma 2, if $x_0 \neq 0$ then the nonlinear element must be asymmetric. The reverse direction of the proof goes in the same manner using Lemma 2. ∎

4 IDENTIFICATION BY USE OF SELF-OSCILLATIONS (IS–O)

Self-oscillations are often considered a malicious effect in control systems. However, self-oscillations can sometimes be used to determine systems's parameters. In these cases, nonlinear elements are intentionally introduced in the closed loop in order to induce self-oscillations.

The concept of identification by use of self-oscillations was introduced about 25 years ago when Åström and Hägglund in [1] derived a so-called ATV (autotuning variation) method used for system identification. The method was presented as simple and appropriate for in situ identification. The method is based on using a relay-feedback to bring the system to self-oscillations. Then Luyben in [14] used this method in chemical industry to identify a transfer function of extremely nonlinear systems (distillation columns). Since then, inducing self-oscillations proved to be an efficient tool for controller tuning in processes and for process identification, [11], [5], especially in pharmaceutical industry. There are no records of this methodology being used for marine vehicles apart from the work from the authors. The work that is presented in this paper demonstrates the use of the IS–O method on a class of nonlinear models which can be used to describe dynamics of underwater vehicles.

A general strictly proper ($n > m$) nonlinear process can be described with

$$f(a_i, x^{(n)}, x^{(n-1)}, ..., x, u^{(m)}, u^{(m-1)}, ..., \dot{u}) = u + \delta$$
(21)

where a_i are process' parameters, x is process output, u process input and δ constant term at the input. If self-oscillations are induced by introducing a nonlinear element, the input to the nonlinear element can be written as

$-x(t) = x_0 + X_m \sin(\omega t)$ where X_m and ω are magnitude and frequency of the established self-oscillations, respectively and x_0 is the biased component caused by δ. Without the loss of generality, the closed loop reference is assumed $x_{ref} = 0$. The derivatives of the process' output are

$$
\begin{aligned}
x &= x_0 + X_m \sin(\omega t) \\
\dot{x} &= X_m j\omega \sin(\omega t) \\
&\vdots \\
x^{(k)} &= X_m (j\omega)^k \sin(\omega t)
\end{aligned}
\tag{22}
$$

and the process can be developed into a Fourier series. Keeping only the first harmonic leads to

$$
[f_R(a_i, x_0, X_m, \omega) + j f_I(a_i, x_0, X_m, \omega)] x^* = u + \delta.
\tag{23}
$$

The term $f_0(a_i, x_0, X_m, \omega)$ of the process is considered to be 0 for the sake of simplicity. Unity feedback implies that

$$
u(t) = -F_0(x_0, X_m) - G_N(x_0, X_m) \cdot x^*
\tag{24}
$$

where $F_0(x_0, X_m)$, and $G_N(x_0, X_m) = P_N(x_0, X_m) + jQ_N(x_0, X_m)$ are parameters of the describing function of the nonlinear element and do not depend on frequency of self-oscillations if the nonlinearity is static. Combining (23) with (24), an equation is obtained which can be separated in an oscillatory component and static component forming two equations given with (25).

$$
\begin{aligned}
f_R + j f_I &= -P_N - j Q_N \\
F_0 &= \delta
\end{aligned}
\tag{25}
$$

From here, three equations can be determined and they can be used to calculate unknown parameters of the process.

Two case studies will be analyzed in this paper. The first, given with (26), is a linear first-order differential equation with an integrator. The second case study, given with (28), is a nonlinear first order differential equation with an integrator, where the nonlinearity can be interpreted as linear drag $\beta_{xx} \cdot |\dot{x}(t)|$. Both equations have a bias term δ included. The assumption is made that δ is constant, therefore it can be observed as one of the unknown parameters of the system.

Case study 1 (Constant drag)

This case study is given with (26) and it will also be referred to as the "constant damping" or the "constant drag" case, because damping of the equation is given with β_x.

$$
\alpha \ddot{x}(t) + \beta_x \dot{x}(t) = \delta + u(t)
\tag{26}
$$

Substituting (24) and (22) into (26) gives the following equation

$$
\alpha X_m (j\omega)^2 \sin(\omega t) + j\beta_x X_m \omega \sin(\omega t) = \\
\delta + [-F_0 - (P_N + jQ_N) X_m \sin(\omega t)] \quad ,
$$

with $F_0 = F_0(x_0, X_m)$, $P_N = P_N(x_0, X_m)$ and $Q_N = Q_N(x_0, X_m)$. From here, three equations that describe the unknown parameters can be derived:

$$
\begin{aligned}
\alpha &= \frac{P_N(x_0, X_m)}{\omega^2} \\
\beta_x &= -\frac{Q_N(x_0, X_m)}{\omega} \\
\delta &= F_0(x_0, X_m)
\end{aligned}
\tag{27}
$$

Case study 2 (Linear drag)

This case study is given with (28) and it will also be referred to as the "linear damping" or the "linear drag" case, because damping of the equation is given with $\beta_{xx} \cdot |\dot{x}(t)|$.

$$
\alpha \ddot{x}(t) + \beta_{xx} |\dot{x}(t)| \dot{x}(t) = \delta + u(t)
\tag{28}
$$

Substituting (24) and (22) into (28) gives the following equation

$$
\alpha X_m (j\omega)^2 \sin(\omega t) + j\beta_{xx} X_m^2 \omega^2 |\sin(\omega t)| \sin(\omega t) = \\
\delta + [-F_0 - (P_N + jQ_N) X_m \sin(\omega t)] ,
$$

with $F_0 = F_0(x_0, X_m)$, $P_N = P_N(x_0, X_m)$ and $Q_N = Q_N(x_0, X_m)$. Further development of the nonlinear term to the Fourier series gives

$$
|\sin(\omega t)| \sin(\omega t) \approx \frac{3\pi}{8} \sin(\omega t) ,
$$

and finally, three equations that describe the unknown parameters can be written::

$$
\begin{aligned}
\alpha &= \frac{P_N(x_0, X_m)}{\omega^2} \\
\beta_{xx} &= -\frac{3\pi}{8} \frac{Q_N(x_0, X_m)}{X_m \omega} \\
\delta &= F_0(x_0, X_m)
\end{aligned}
\tag{29}
$$

4.1 Benchmark example: Relay with hysteresis

The most commonly used nonlinearity for inducing self-oscillations in practice is a two-position relay with hysteresis, [21]. Some work related to using relay for identification of process parameters can be found in [9], [10], [26], [25], [24]. Some of the main reasons why this element is commonly used are that

- every system whose Nyquist characteristic passes through the II quadrant can be caused to oscillate (this comes as direct consequence of the Goldfarb method, [23]),

- it is insensitive to noise, and
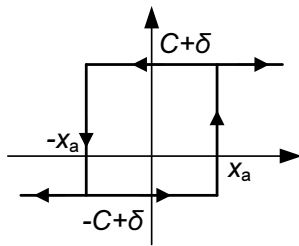
- it is easily implementable.

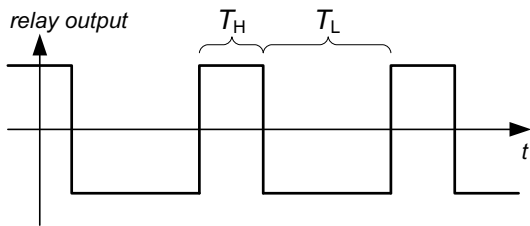Fig. 5. Asymmetric two-position relay with hysteresis

Fig. 6. Asymmetric output from the relay with hysteresis

Fig. 7. Illustration of false switching in discrete-time systems

Fig. 5 shows the asymmetric two-position relay with hysteresis where C is relay output, x_a is hysteresis width and δ is the bias term which causes the asymmetric oscillations at the output of the relay shown in Fig. 6. The describing function parameters for such nonlinearity can be determined by using (14) and are as follows:

$$Q_N = -\frac{4Cx_a}{\pi X_m^2} \qquad (30)$$

$$P_N = \frac{2C}{\pi X_m}\left[\sqrt{1-\left(\frac{x_a-x_0}{X_m}\right)^2} + \sqrt{1-\left(\frac{x_a+x_0}{X_m}\right)^2}\right] \qquad (31)$$

It is worth noting that the imaginary part of the describing function, $Q_N(x_0, X_m)$, is in fact not a function of x_0. The unbiased describing function is obtained if $x_0 = 0$. The static term of the describing function can also be determined and it is given with (32).

$$F_0 = C\frac{T_H - T_L}{T_H + T_L} \qquad (32)$$

To sum up, the terms for identifying unknown parameters of the two case studies when the nonlinear element is in the closed loop, can be found in Table 3.

4.2 Modification for systems with delays

Delays in systems have great influence on quality of control. They are often present and seldom negligible. Some research h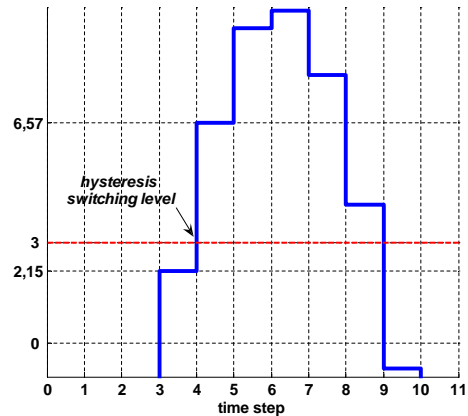as been done on autotuning of systems with time delays, but they were mostly based on inserting an additional time delay in order to shift the system in phase and therefore obtain different frequency points for identification. In this paper, time delay will be treated as a known part of the system, and its influence has to be compensated for. The influence of time delays is rather obvious in systems forced into self-oscillations: they have greater magnitude and smaller frequency of oscillations. If the system with a delay is to be identified, the delay should be taken into account. Let's suppose that the general nonlinear process (21) has a time delay T_d at the input, i.e. $u + \delta \doteq u(t - T_d) + \delta(t - T_d)$. Then (23) can be rewritten as

$$\begin{array}{rcl} f_R + jf_I & = & (P_N + jQ_N)\,e^{-j\omega T_d} \\ F_0 & = & \delta \end{array} \qquad (33)$$

This modification can be observed as rotation of the original vector of the describing function by an angle $-\omega T_d$. In other words, same equations as for the system without process delay can be used, only the modified describing function parameters P_N^* and Q_N^* have to be calculated using (34).

$$\left[\begin{array}{c} P_N^* \\ Q_N^* \end{array}\right] = \left[\begin{array}{cc} \cos\omega T_d & \sin\omega T_d \\ -\sin\omega T_d & \cos\omega T_d \end{array}\right]\left[\begin{array}{c} P_N \\ Q_N \end{array}\right]. \qquad (34)$$

4.3 Modification for discrete-time systems

When the IS-O method is used in practice, the process is usually computer-controlled. Therefore a slight modification of the procedure has to be done.

Let's say that the nonlinear element which caused the self-oscillations in the system is a relay with hysteresis with $x_a = 3$. This means that it should switch when the input signal has value 3. It could happen that at some time step k the input is 2.15 and at the following time step $k+1$ it is 6.57, as shown in Fig. 7. Since at the moment k the

Table 3. Formulae for determining unknown parameters using IS-O method with relay with hysteresis

Case study 1 (constant drag)	Case study 2 (linear drag)
$\alpha_x = \frac{P_N(x_0, X_m)}{\omega^2} = \frac{2C}{\pi} \frac{1}{\omega^2 X_m} \left[\sqrt{1 - \left(\frac{x_a - x_0}{X_m}\right)^2} + \sqrt{1 - \left(\frac{x_a + x_0}{X_m}\right)^2} \right]$	
$\beta_x = -\frac{Q_N(X_m)}{\omega} = \frac{4Cx_a}{\pi} \frac{1}{\omega X_m^2}$	$\beta_{xx} = -\frac{3\pi}{8} \frac{Q_N(X_m)}{X_m \omega^2} = \frac{3Cx_a}{2} \frac{1}{\omega^2 X_m^3}$

$$\delta = C \frac{T_H - T_L}{T_H + T_L}$$

input to the relay has not yet reached the switching value, it will switch at the moment $k + 1$. In other words, this is equivalent to hysteresis parameter x_a having the value $x_a^* = 6.57$, which is more than double the assumed value, therefore false results can be expected. It can also happen that the switching occurs exactly at the desired moment, resulting in accurate identification. Since it cannot be known a priori weather the chosen hysteresis parameters will give satisfactory results, the only way is to perform the correction of the hysteresis width (determine real switching levels x_a^*), after the experiment has been performed. With smaller sampling times, the chances of hysteresis switching at $x_a^* \gg x_a$ become smaller. However, sampling time is usually not something that can be altered, therefore the proposed modification is necessary.

5 IMPLEMENTATION OF IS–O TO UNDERWATER VEHICLES

5.1 System description

The vehicle that was used to implement the proposed identification by use of self oscillations method is a Video-Ray ROV shown in Fig. 8(a). Its dimensions are 355mm x 228mm x 215mm and it weighs 3.5kg. Heading sensor is a magnetic compass with $2°$ quantization. In addition, it is equipped with a depth pressure-based sensor. The vehicle is actuated using a port, starboard and vertical thruster. The schematic representation of thruster locations is shown in Fig. 8(b) from where it follows that the thruster allocation matrix (only for port and starboard thrusters) can be written using (35).

$$\begin{bmatrix} X \\ N \end{bmatrix} = \begin{bmatrix} 1 & 1 \\ d & -d \end{bmatrix} \begin{bmatrix} \tau^1 \\ \tau^2 \end{bmatrix} \quad (35)$$

Determining the static characteristic of a thruster, i.e. the relation between the exerted thrust τ^i and the thruster control signal (voltage n^i in this case) is called thruster
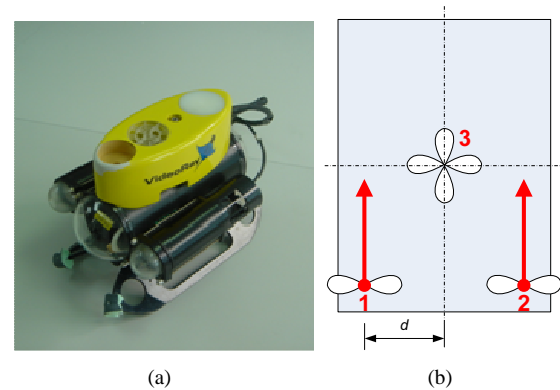

Fig. 8. a) VideoRay ROV and b) thruster distribution

mapping. The simplest way to perform this mapping is to induce vehicle motion in such a way that the pull-force of the vehicle can be recorded by a dynamometer, as shown in Fig. 9(a). After a series of such experiments, for different input signals, the results shown in Fig. 9(b) have been obtained, where the dots represent measured values and the full line gives the interpolated curve, given with (2).

The ROV is connected to the surface computer via tether as it is shown in Fig. 10. All the control algorithms are calculated and executed on the surface and sent to the ROV using the RS - 232 interface. The schematic representation of the complete system that was used for identification is shown in Fig. 11. Yellow blocks represent the communication with the ROV. *COMM 1* is communication from the surface computer towards the vehicle and is modeled as one discretization step delay ($T_d = 0.1$s). Block *COMM 2* is modeled in the same manner and it represents the communication delay from the ROV towards the surface where the heading data is collected. The blue block entitled "VideoRay ROV" represents the vehicle itself. The signals inside this block are virtual and are marked with a
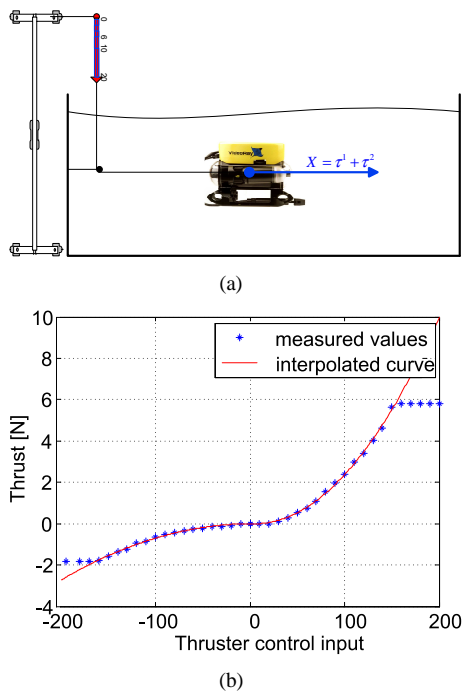
(a)

(b)

Fig. 9. Thruster mapping a) experiment and b) results for VideoRay ROV

hash symbol. The parameters that are to be identified using the IS-O method are the parameters of the dynamic yaw model of the vehicle. However, the vehicle demonstrates some nonlinear behaviors which must be detected prior to the initiation of the IS-O method. One of these nonlinearities is the relation between the thruster input voltage (n^1 and n^2) and thrust itself (τ^1 and τ^2). This relation has been described before and is schematically represented as $f(x)$ in Fig. 11. The *thruster allocation* block is given with (35). It has been noted that small voltage applied to the thrusters will not cause them to rotate, mainly because of friction. This effect has been modeled using the dead zone blocks.

Now that these static nonlinearities and allocations have been defined, they can be compensated for before the iden-
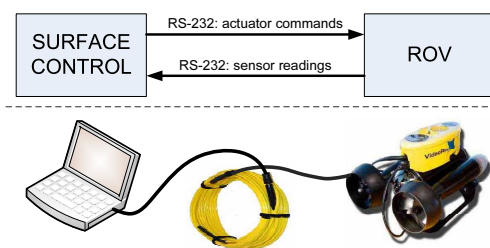

Fig. 10. Connection of the ROV to the surface control unit

tification procedure is initiated. The green *a priori compensation* block has the purpose to compensate for as many nonlinearities in the system as possible. The dead zone inherent to thrusters is avoided by adding a constant signal so that the thrusters are rotating even at small input voltages. The nonlinear thruster characteristic can easily be compensated by applying the inverse of identified characteristic, $f^{-1}(x)$. In order to control the vehicle by sending it the yaw moment (N) command, inverse thruster allocation has to be performed. This block presents the matrix inversion of (35). In other words, the complete system, from the input yaw moment N through the output heading ψ can be modeled with (36), in concordance to (6).

$$\alpha_r \ddot{\psi} + \beta\left(\dot{\psi}\right) \cdot \dot{\psi} = N\left(t - 2T_d\right) + \tau_{NE} \qquad (36)$$

τ_{NE} presents the external disturbance that is mainly caused by the tether. This disturbance is assumed to be constant and has to be estimated during the identification process. Another assumption is that drag is either dominantly constant or dominantly linear. This means that general drag $\beta\left(\dot{\psi}\right)$ can obtain one of the two values:

$$\beta\left(\dot{\psi}\right) = \begin{cases} \beta_r & \text{for constant drag} \\ \beta_{rr}\left|\dot{\psi}\right| & \text{for linear drag} \end{cases} \, .$$

Since it is not known a priory what kind of model best describes the VideoRay ROV, a methodology for determining which of these models suits the vehicle best will be developed and elaborated later on.

5.2 Quantization levels

The quantization can greatly influence the quality of the identified system. Different compasses can have different quantization levels, and based on the quality of the compass, identification results can differ. The same goes for other sensors which can be used to determine vehicle's model based on the self-oscillation experiments.

Using the formulae in Table 3, the percentual difference in the identified parameters can be found in relation to percentual difference of the quantization interval (ΔX_m) and the magnitude of self-oscillations (X_m). These error estimates are given with (37), (38) and (39).

$$\frac{\Delta \alpha_x}{\alpha_x} = \frac{2 - \left(\frac{X_m}{x_a}\right)^2}{\left(\frac{X_m}{x_a}\right)^2 - 1} \frac{\Delta X_m}{X_m} \qquad (37)$$

$$\frac{\Delta \beta_x}{\beta_x} = -2\frac{\Delta X_m}{X_m} \qquad (38)$$

$$\frac{\Delta \beta_{xx}}{\beta_{xx}} = -3\frac{\Delta X_m}{X_m} \qquad (39)$$
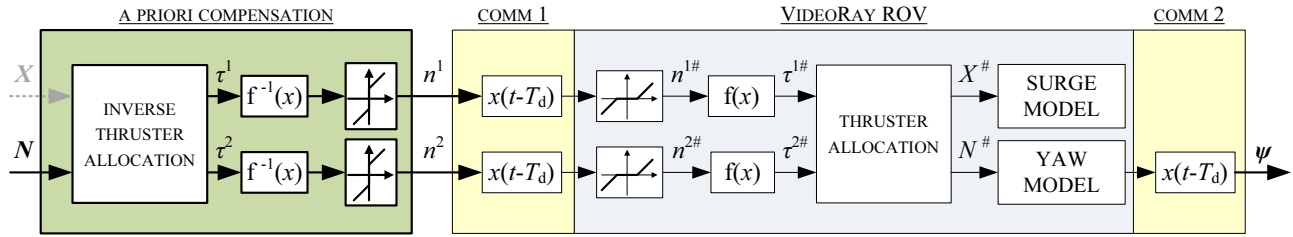
Fig. 11. Schematic representation of the complete model

It is clear that the percentual errors in determining β_x and β_{xx} caused by quantization are constant. The absolute errors in these parameters however, can be minimized if the experiments are performed with greater magnitude of self-oscillations (minimizing the percentual error of magnitude).

5.3 Experimental results

The self-oscillation experiments were performed in the Laboratory for Underwater Systems and Technologies, Faculty of Electrical Engineering and Computing, University of Zagreb. The Laboratory is equipped with a circular pool 1.5 m deep, which made it impossible to conduct the heave degree of freedom tests on the real vehicle. However, extensive experiments have been carried out on identifying the yaw degree of freedom.

An example of responses during one experiment are shown in Fig. 12. First plot gives the input to the relay, $\psi_{ref} - \psi$, while the second plot gives relay output N. Red circles represent maxima of the oscillations, green dots minima and yellow stars represent the moments in which relay switching occurred.

For the experiment to be successful, self-oscillations have to be obtained. A condition which has to be fulfilled for this is given with (40). This comes as a direct consequence of the domain of real part of the describing function of the asymmetric relay with hysteresis (31). An example of the relay parameters set inappropriately is given in Fig. 13, where hysteresis width was chosen to be $x_a = 0$.

$$\frac{x_a^* - x_0}{X_m} < 1 \qquad (40)$$

Once the data have been obtained the following procedure is executed:

1. Calculate average magnitude X_m and average frequency ω of self-oscillations.

2. Calculate average hysteresis switching level x_a^*. x_a^* will be bigger than the preset one (x_a) because of the discrete nature of the signal (see Section 4.3).
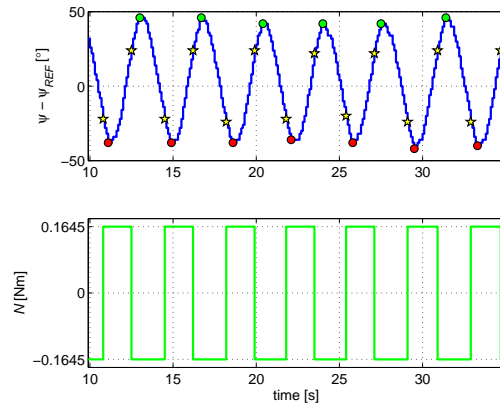

Fig. 12. Example of responses during the IS-O method

3. Calculate average bias of the input signal x_0. The existence of x_0 means that external disturbance was present during the experiment (tether in the specific case).

4. Check condition (40). If false, repeat experiment with different relay parameters and go to 1.

5. Calculate vehicle parameters using the formulae in Table 3. The delay is to be compensated using (34).

The self-oscillation parameters were changed by varying two relay parameters: relay output N and hysteresis width x_a. All together, 19 experiments were performed and the results can be found in Table 4. Based on the standard deviations of obtained β_x and β_{xx} it can be concluded that the linear drag model fits the data better with a standard deviation between the measurements of 14.84%. For better representation, Fig. 14 gives relative errors of parameters $\alpha_{r,i}$, $\beta_{r,i}$ and $\beta_{rr,i}$ calculated in the i-th experiment with regard to the obtained mean values $\bar{\alpha}_r = \frac{\sum_{i=1}^{19} \alpha_{r,i}}{19}$, $\bar{\beta}_r = \frac{\sum_{i=1}^{19} \beta_{r,i}}{19}$ and $\bar{\beta}_{rr} = \frac{\sum_{i=1}^{19} \beta_{rr,i}}{19}$, respectively. Green circles in first plot show $p_{\alpha_{r,i}} = \left| \frac{\alpha_{r,i} - \bar{\alpha}_r}{\bar{\alpha}_r} \right| \cdot 100\%$, and in the second plot green diamonds show $p_{\beta_{r,i}} = $
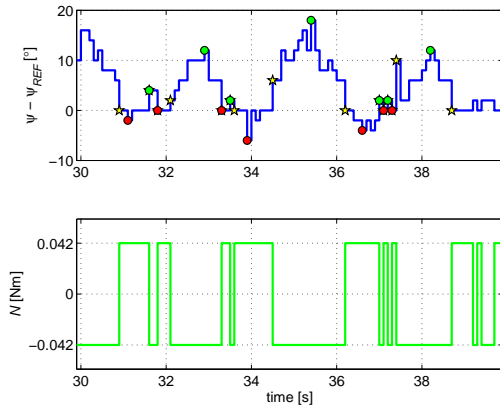
Fig. 13. Example of responses during the IS-O method when conditions for inducing self-oscillations are not fulfilled ($x_a = 0$)
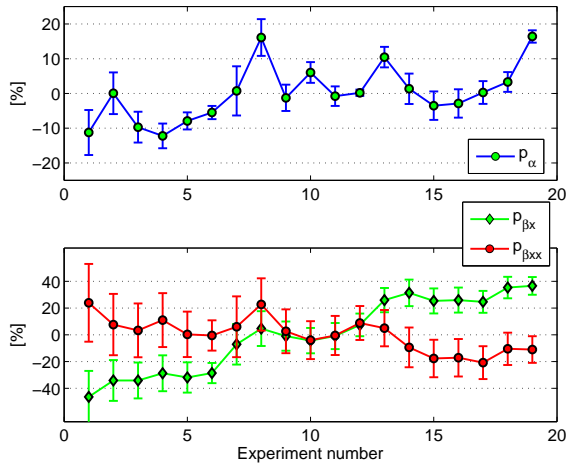

Fig. 14. Relative errors and quantization confidence bounds for identified parameters

$\left| \frac{\beta_{r,i} - \bar{\beta}_r}{\bar{\beta}_r} \right| \cdot 100\%$ and red circles $p_{\beta_{rr,i}} = \left| \frac{\beta_{rr,i} - \bar{\beta}_{rr}}{\bar{\beta}_{rr}} \right| \cdot 100\%$. The confidence bounds are calculated based on the error which can occur due to quantization effects, and they are calculated by using formulae (37), (38) and (39). It is easily seen that confidence bounds get smaller as the magnitude of self-oscillations gets bigger. This leads to the conclusion that self-oscillations experiments should be run with higher oscillating magnitudes in order to minimize the error caused by quantization effects. These experiments show that IS-O method can be applied to identify underwater vehicle mathematical model parameters with sufficient precision.

However, the point of IS-O method is not to perform a great number of experiments in order to determine the

model of the vehicle. The experimental data have shown that model parameters can be determined accurately from a single experiment. The methodology on how to determine which model structure is more appropriate is described in the following section.

5.4 Deciding on the appropriate model

The extensive experiments have shown that the most appropriate model for the vehicle is the one with linear drag (nonlinear model). In other words, the equation for calculating the drag which should be used is given with (29).

However, this cannot be known if only one self-oscillation experiment has been conducted. That is why an additional experiment, with different relay parameters should be conducted. From the first experiment α_{x1}, β_{x1}, β_{xx1} are obtained, and from the second α_{x2}, β_{x2}, β_{xx2}. Standard deviations can be calculated as

$$
\begin{aligned}
\sigma_{\alpha_x}\% &= \left| \frac{\alpha_{x1} - \alpha_{x2}}{\alpha_{x1} + \alpha_{x2}} \right| \cdot 100\% \\
\sigma_{\beta_x}\% &= \left| \frac{\beta_{x1} - \beta_{x2}}{\beta_{x1} + \beta_{x2}} \right| \cdot 100\% \\
\sigma_{\beta_{xx}}\% &= \left| \frac{\beta_{xx1} - \beta_{xx2}}{\beta_{xx1} + \beta_{xx2}} \right| \cdot 100\%.
\end{aligned}
\tag{41}
$$

Theoretically, $\sigma_{\alpha_x}\%$ should be 0. In real experiments it will have some value, which can be interpreted as measurement uncertainty. The criterion for determining which model best describes the vehicle is given with (42), where λ is a parameter which determines the robustness of the decision making.

$$
\sigma_{\beta_x}\% - \sigma_{\beta_{xx}}\% \begin{cases} > & \lambda & \Rightarrow \text{linear drag } (\beta_{xx}) \\ < & -\lambda & \Rightarrow \text{constant drag } (\beta_x) \\ \in & [-\lambda, \lambda] & \Rightarrow \text{no decision} \end{cases}
\tag{42}
$$

Depending on robustness parameter λ, four different criteria were tested:

1. $\lambda = 0$ is the least robust criterion ensuring that any pair of measurements will result in a decision on the model, even though the difference between standard deviations is small. This criterion may lead to wrong decisions.

2. $\lambda = \sigma_{\alpha_x}\%$ is a criterion which includes the measurement uncertainty described by the standard deviation of $\alpha_\%$. Robustness in this case is increased and there is a margin in which decision might not be made.

3. $\lambda = \sigma_{\alpha_x}\% + 5\%$ is a criterion with increased robustness. The margin of not making a decision is also increased.

4. $\lambda = \sigma_{\alpha_x}\% + 10\%$ is a criterion with increased robustness where it is demanded that the difference between

Table 4. Experimental results obtained from the Videoray ROV yaw DOF

Exp. No.	N [Nm]	x_a^* [deg]	X_m [deg]	x_0 [deg]	$T = \frac{1}{\omega}$ [s]	α_r $\left[\frac{\mathrm{Nms}^2}{\mathrm{deg}} \cdot 10^{-4}\right]$	β_r $\left[\frac{\mathrm{Nms}}{\mathrm{deg}} \cdot 10^{-4}\right]$	β_{rr} $\left[\frac{\mathrm{Nms}^2}{\mathrm{deg}^2} \cdot 10^{-5}\right]$
1	2.10	10.29	20.6	2	4.26	5.05	6.4	2.48
2	3.85	11	26.17	1.17	3.82	5.69	7.87	2.16
3	3.85	15	29.8	7.8	4.18	5.14	7.87	2.07
4	3.85	16.84	29.78	2.22	4.14	4.99	8.52	2.22
5	3.85	21.20	35.25	1.25	4.64	5.24	8.14	2.01
6	3.85	41.07	53	3.86	6.6	5.38	8.53	1.99
7	8.23	6.58	26.36	3.8	2.69	5.73	11.11	2.12
8	8.23	12.21	30.69	1.62	3.21	6.6	12.51	2.46
9	8.23	17.73	36.57	2.86	3.39	5.62	11.84	2.06
10	8.23	21.92	42.25	4.75	3.79	6.03	11.44	1.92
11	8.23	22.37	41.08	2.62	3.68	5.64	11.85	1.99
12	8.23	31.29	47.17	1.5	4.27	5.70	12.85	2.18
13	12.6	22.42	44.09	1.55	3.28	6.28	15.07	2.10
14	16.98	13.12	40.33	2.17	2.48	5.76	15.72	1.81
15	16.98	14.25	42.73	3.67	2.5	5.49	14.99	1.65
16	16.98	14.33	42.73	2.36	2.51	5.52	15.07	1.66
17	16.98	19.83	48.88	2.29	2.77	5.7	14.91	1.59
18	16.98	23.6	49.67	2.78	2.93	5.88	16.19	1.79
19	16.98	34	60.33	2.67	3.51	6.62	16.34	1.78
$\overline{x}$						5.69	11.96	2
$\frac{\sigma_x}{\overline{x}} \cdot 100\%$						8.07	27.38	12.48

standard deviations be significantly different. In this case the decision that is made can be considered correct, but the path to making a decision may require more measurements being taken.

Based on the experiments which were performed, the conclusion is made that the model with linear drag describes the system better than the one with constant drag. Among the 19 experiments, pairs were taken in such a way that one pair must have different relay outputs N. This is common, since the two experiments that are performed to decide on the model should be as different as possible. This condition leads to 131 different combinations of pairs. All four criteria have been tested and the results are shown in Fig. 15, where dark green represents the number of pairs when the conclusion was correctly made, light green the number of pairs when the conclusion was falsely made and in yellow the number of pairs where the conclusion could not be made.

It is clear from Fig. 15 that criterion 1 always caused the decision to be made, and in almost 90% of pairs the conclusion was made correctly. In about 7 times less cases, the conclusion was false. When using criterion 2, the margin of no decision is introduced and for a number of experi-

ments the decision could not be made (below 10%). However, in this case, the number of correct decisions is 8 time bigger then wrong decisions. By increasing the margin of decision (criteria 3 and 4) the number of cases without decision increases, but the number of pairs with correct decision gets 12 (criterion 3) and even 37 (criterion 4) times bigger.

5.5 Discussion on identifying heave and surge models

For identification of a heave model, depth sensor must be applied. The equation which describes heave motion is given with (43) where $\beta(\dot{z})$ can be either β_w or $\beta_{ww}|\dot{z}|$, just like in the yaw case.

$$\alpha_w \ddot{z} + \beta(\dot{z}) \cdot \dot{z} = Z(t - 2T_d) + \tau_{ZE} \qquad (43)$$

However, in (43) τ_{ZE} presents the external disturbance and difference between weight W and buoyancy B of the vehicle. The difference is usually dominant in comparison to the external disturbance that is mainly caused by the tether, which is why greater asymmetry in self-oscillations should be expected during IS-O experiments, [17]. Special attention should be paid to quantization errors since depth sensors often give rough measurements.
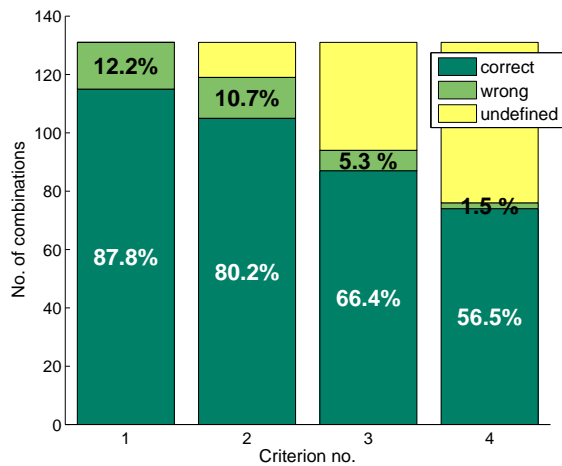
Fig. 15. Number of cases when the conclusion was correct, false or undefined

The identification of the surge model is commonly conducted using a Doppler velocity logger (DVL), which gives surge speed as output (among other speeds). This means that the model to be identified would be of the first order without an integrator. However, the same procedure as in yaw case can be applied if the integral of measured surge speed $u^\diamond = \int u \, dt$ is introduced to the relay input. Then the surge model can be described with (44) where $\beta (\dot{u}^\diamond)$ can be either β_u or $\beta_{uu} |\dot{u}^\diamond|$, just like in the yaw case.

$$\alpha_u \ddot{u}^\diamond + \beta (\dot{u}^\diamond) \cdot \dot{u}^\diamond = X (t - 2T_d) + \tau_{XE} \qquad (44)$$

6 CONCLUSIONS

The use of identification procedures based on self-oscillations has been applied to underwater vehicles in this paper and it has proven to be time preserving (in comparison to conventional identification methods), easily applicable and implementable, and computationally not demanding.

The IS-O method was applied by inserting a symmetric nonlinear element in the closed loop right before the UV. In the starting part, special attention was dedicated to self-oscillations, which occur in closed loop systems consisting of a nonlinear element and an astatic process (linear and nonlinear). It has been proven that in such systems self-oscillations are symmetric if the nonlinear element is symmetric, regardless of the reference input. In addition to that, the proof is given that asymmetric oscillations can occur if and only if the nonlinear element is asymmetric. This proof is important since external disturbance in underwater vehicles appears exactly at the output of the nonlinear element (input to the UV), forming an asymmetric nonlinear characteristic.

The proposed IS-O method was derived for identifying processes which exhibit asymmetric self-oscillations, for the purpose of generality. It was also shown that the disturbance in the system does not correlate to the identified drag of the vehicle. In addition to that, the IS-O method is extended to cover the systems with delays.

Extensive IS-O experiments have been performed on yaw DOF of VideoRay ROV showing that the best fitting model is nonlinear. However, the key point of IS-O method is to perform only one experiment to determine the model and these multiple experiments have shown that each experiment gives accurate model parameter estimations. In order to determine the most appropriate structure of the model, a practical decision-making scheme was presented and applied to the real ROV. in addition to that, estimates of errors due to quantization have been given and the conclusion was raised that these errors decrease with the increase of magnitude of self-oscillations.

In the final part, suggestions for applying the proposed IS-O method on other degrees of freedom of underwater vehicles are stated.

ACKNOWLEDGMENT

REFERENCES

[1] K. J. Åstrom and Hagglund, **Automatic tuning of simple regulators with specifications on phase and amplitude margins**, in Proeedings of the NGCUV'08 Conference, 20:645, 1984.

[2] M. Caccia, G. Casalino, R. Cristi, and G. Veruggio, **Acoustic motion estimation and control for an unmanned underwater vehicle in a structured environment**, Control Engineering Practice, vol. 6, pp. 661–670, 1998.

[3] M. Caccia, G. Indiveri, and G. Veruggio, **Modelling and identification of open-frame variable configuration underwater vehicles**, IEEE Journal of Ocean Engineering, vol. 25, no. 2, pp. 227–240, 2000.

[4] M. Caccia and G. Veruggio, **Guidance and control of a reconfigurable unmanned underwater vehicle**, Control Engineering Practice, vol. 8, no. 1, pp. 21–37, 2000.

[5] R.C. Chang, S.H. Shen, and C.C. Yu, **Derivation of transfer function from relay feedback systems**, Industrial and Engineering Chemistry Research, vol. 31, no. 3, pp. 855–860, 1992.

[6] H.-H. Chen, **Vision-based tracking with projective mapping for parameter identification of remotely operated vehicles**, Ocean Engineering, vol. 36, pp. 983–994, 2008.

[7] T.I. Fossen, **Guidance and Control of Ocean Vehicles**, John Wiley & Sons, New York, NY, USA, 1994.

[8] G.C. Karras and K.J. Kyriakopoulos, **Localization of an underwater vehicle using an IMU and a laser-based vision system**, in Proceedings of the 15th Mediterranean Conference on Control and Applications, 2007.

[9] I. Kaya and D. P. Atherton, **Parameter estimation from relay autotuning with asymmetric limit cycle data**, Journal of Process Control, vol. 11, pp. 429, 2001.

[10] H. J. Kwak, W. S. Sung, and I.-B. Lee, **On-line process identification and autotuning for integrating processes**, Industrial and Engineering Chemistry Research, vol. 36, pp. 5329–5338, 1997.

[11] W. Li, E. Eskinat, and W. L. Luyben, **An improved autotune identification method**, Industrial and Engineering Chemistry Research, vol. 30, pp. 1530, 1991.

[12] L. Ljung, **System Identification - Theory for the User**, Second edition, Prentice Hall, 1999.

[13] E. López, F.J. Velasco, E. Moyano, and T.M. Rueda, **Full-scale manoeuvering trials simulation**, Journal of Maritime Research, vol. 1, no. 3, pp. 37–50, 2004.

[14] W. L. Luyben, **Derivation of transfer functions for highly nonlinear distillation columns**, Industrial and Engineering Chemical Research, vol. 26, pp. 2490, 1987.

[15] N. Mišković, Z. Vukić, and M. Barišić, **Identification of coupled mathematical models for underwater vehicles**, in Proceedings of the OCEANS'07 Conference, 2007.

[16] N. Mišković, Z. Vukić, and M. Barišić, **Identification of Underwater Vehicles for the Purpose of Autopilot Tuning - Intelligent Underwater Vehicles**, InTech Education and Publishing, Vienna, 2009.

[17] N. Mišković, Z. Vukić, and E. Omerdić, **Control of UUVs based upon mathematical models obtained from self-ocillations experiments**, in Proceedings of the NGCUV'08 Conference, 2008.

[18] A. Netushil, **Theory of Automatic Control**, Mir Publishers, Moscow, 1978.

[19] E. Omerdić, **Thruster fault diagnosis and accommodation for overactuated open-frame underwater vehicles**, PhD thesis, University of Wales, Newport, United Kingdom, 2004.

[20] P. Ridao, A. Tiano, A. El-Fakdi, M. Carreras, and A. Zirilli, **On the identification of non-linear models of unmanned underwater vehicles**, Control Engineering Practice, vol. 12, pp. 1483–1499, 2004.

[21] Y. Z. Tsypkin. **Relay Control Systems**, Cambridge University Press, Cambridge, UK, 1984.

[22] Z. Vukić and Lj. Kuljača, **Automatic Control - Analysis of Linear Systems**, Kigen, Zagreb, 2005. In Croatian.

[23] Z. Vukić, Lj. Kuljača, D. Đonlagić, and S. Tešnjak, **Nonlinear Control Systems**, Marcel Dekker, New York, 2003.

[24] L. Wang, M. L. Desarmo, and W. R. Cluett, **Real-time estimation of process frequency response and step response from relay feedback experiments**, Automatica, vol. 35, pp. 1427, 1999.

[25] Q. G. Wang, C. C. Hang, and Q. Bi, **Process frequency response estimation from relay feedback**, Control Engineering Practice, vol. 5, no. 9, pp. 1293, 1997.

[26] Q. G. Wang, C. C. Hang, and B. Zou, **Low order modeling from relay feedback**, Industrial and Engineering Chemistry Research, vol.36, pp. 375–381, 1997.

Nikola Mišković obtained his diploma from the University of Zagreb, Faculty of Electrical Engineering and Computing, Zagreb, Croatia in 2005. During his studies he was awarded three "Josip Loncar" recognitions for success in studies by the Faculty. He is currently pursuing the Ph.D. degree at the same university where he is employed as a Teaching and Research Assistant. In 2008, he was a guest researcher at Consiglio Nazionale delle Ricerche in Genoa, Italy. He is a member of the Laboratory for Underwater Systems and Technologies at the University of Zagreb and a member of IEEE Oceanic engineering society. His current research interests include identification, control and guidance of unmanned marine vehicles, nonlinear system theory and its applications.

Zoran Vukić is professor of Control Engineering at the University of Zagreb, Faculty of Electrical Engineering and Computing. Between 1992 and 1996 he has been the Head of the Department of Control and Computer Engineering. He specialized in control at Royal Institute of Technology, Stockholm, Sweden in 1984. He has been a Fulbright fellow at Vanderbilt University in 1985 and a Visiting professor there in 1985/86. His specific interests have been adaptive control, robust control, identification, nonlinear control, fault tolerant control and reconfigurable control. He is currently working in the area of intelligent, reconfigurable and fault tolerant control for marine and underwater vehicles. He is member of IEEE Control Systems Society and Oceanic Engineering Society, member of IFAC TC on Marine Systems and TC on Adaptive Control and Learning, and member of AUSI (Autonomous Underwater Systems Institute, US) consortium. He is author or co-author of four books and more than 100 scientific papers. He is a recipient of "Donald Maxwell Award" of Society of Maritime Industries for the best paper in 2003 and recipient of the "J. J. Strossmayer" award by the Croatian Academy of science and art for the best book published in 2004. He is a member of editorial board of Croatian journal "Brodogradnja" (Shipbuilding) and Unmanned Systems Editor of the "Journal of Intelligent and Robotic Systems" (JINT) by Springer.

Matko Barišić was born in 1980 and obatined his diploma in Electrical Engineering (Control Engineering) from the University of Zagreb, Faculty of Electrical Engineering and Computing in 2003. He has been enrolled in the Ph.D. course in Electrical Engineering (Control Engineering) from the University of Zagreb, Faculty of Electrical Engineering and Computing since June 2004.

His topics of interest include applications of vector linear algebra and analysis (calculus) to problems of guidance of underactuated rigid bodies in 6 degrees of freedom, distributed guidance algorithms for coordinated control of autonomous underwater vehicle formations, algorithms for ensuring controllability, robustness and agent forming under communication constraints and optimal estimation.

AUTHORS' ADDRESSES
Nikola Mišković, M.Sc.
Prof. Zoran Vukić, Ph.D.
Matko Barišić, M.Sc.
Laboratory for Underwater Systems and Technologies,
Department of Control and Computer Engineering,
Faculty of Electrical Engineering and Computing,
University of Zagreb,
Unska 3, HR-10000 Zagreb, Croatia
emails: nikola.miskovic@fer.hr,
zoran.vukic@fer.hr, matko.barisic@fer.hr